Springer

Acta Mechanica Sinica

CrossMark click for updates

•RESEARCH PAPER•

Acta Mech. Sin., Vol. 38, 321399 (2022)
https://doi.org/10.1007/s10409-021-09023-z

Research on phosphorus release from resuspended sediment under wind-induced waves in shallow water

Pengda Cheng[1], Xinguang Zhu[1,2], Yi An[1], and Chun Feng[1*]

[1] *Institute of Mechanics, Chinese Academy of Sciences, Beijing 100190, China;*
[2] *School of Engineering Science, University of Chinese Academy of Sciences, Beijing 100049, China*

Received August 11, 2021; accepted October 20, 2021; published online February 10, 2022

Sediment-water interfaces are important interfaces for lakes, which are related to most environmental and ecological problems. Wind-induced waves cause secondary pollution via sediment resuspension. Since the coupling mechanism of water, resuspended sediments, and phosphorus affects the release of phosphorus (P) near the interface, a coupled model was explored for two sediment types with different adsorption-desorption capabilities to examine sediment resuspension and P release. The relationships among wind speed, wave characteristics, sediment distribution and P concentration were obtained. For different sediments, the unit sediment desorption release is negatively correlated with wind speed. When sediments are resuspended under low or moderate wind speed, the P concentration in the overlying water increases abruptly, hampering diffusion. P release exhibits the characteristics of concentrated release in a small region and changes the water environment rapidly.

Phosphorus, Wind-induced waves, Sediment resuspension, Sediment-water interface, Desorption

Citation: P. Cheng, X. Zhu, Y. An, and C. Feng, Research on phosphorus release from resuspended sediment under wind-induced waves in shallow water, Acta Mech. Sin. **38**, 321399 (2022), https://doi.org/10.1007/s10409-021-09023-z

1. Introduction

Water body can be considered as a natural complex composed of water, soluble substances, suspended substances, aquatic organisms and sediments. When contaminants enter the water body, they will be deposited in the sediments and gradually accumulate, forming a sediment layer of certain thickness containing various contaminants. Thus, the sediments form a reservoir of pollutants. When the sediment is resuspended under hydrodynamic conditions, it will release a large number of contaminants and cause secondary pollution to the water body. When external pollution is controlled, the internal release of contaminated sediments becomes more and more obvious. The migration and transformation of contaminants after the resuspension of sediments are deeply related to the movement of sediment in water [1]. The sediment-water interface is one of the most important interfaces in the land surface system. In lakes, almost all instances of environmental pollution and ecological risks are related to the processes occurring at or the effects of the sediment-water interface [2].

The recent research on sediment-water interface transportation is mainly based on observation and experimentation. Fetters et al. [3] used the resuspended metal-contaminated sediments for experiments. Sediment samples were taken from one site in Lake DePue, Illinois (USA) and two sites in Portsmouth Naval Shipyard, Maine (USA) for experiments. They proposed that the short-term (4 h) resuspension of sediments resulted in metal mobilization in water, and the amount of release was related to hydrodynamics, biochemical reactions, and redox reactions. Matisoff et al. [4] proposed that the increased watershed nutrient loading can cause severe algal blooms in Lake Winnipeg (Canada), much of which was associated with suspended particles. The study indicated that surface sediments as high as 7 cm were actively resuspended for more than 23 years before entering the deeper sediments. Lepage et al. [5] analyzed the effects of suspended particulate matter (SPM) dy-

*Corresponding author. E-mail address: fengchun@imech.ac.cn (Chun Feng)
Executive Editor: Xueming Shao

namics and quality on three major dams on the upper Rhône River (France) during a flushing operation in 2012. The study demonstrated that the concentration of SPM during flushing was on average 6-8 times more than that during flood events recorded in 2011-2016. Pivato et al. [6] developed a "point" model to describe the temperature dynamics of the sediment-water continuum driven by vertical energy transfer and found that the heat exchange between water and sediment is crucial for describing sediment temperature but plays a minor role in determining the water temperature. Experiments on sediment-water interface transportation can be classified into those based on static and dynamic methods. The common static experiment is ectopic culture or *in situ* measurement in columnar sediment-water systems or benthic chambers, and the solute transport at the sediment-water interface can be accurately tracked in this type of experiment [7-9]. Two main types of dynamic factors, namely, physical and biological disturbances, affect the sediment-water interface. Hydrodynamic factors affect sediments in layers, while biological disturbances destroy the surface of sediments in points or blocks. The present study deals with the physical disturbance caused by wind-induced waves, which is concerning.

With regard to the effect of wind-induced waves, Zhu et al. [10] simulated the disturbance caused by waves on sediments with a water flume. The results show that phosphorus (P) and ammonia-nitrogen concentrations increased by 20% and 30%, respectively, under large-wave conditions. You et al. [11] simulated sediment resuspension under wind-induced waves with a propeller-type device and revealed that under strong wind conditions, the increment in P in the water body is lower than that under light wind conditions, and nitrogen even tends to decrease. Wu et al. [12] showed that the shear stress of wind-induced waves at the bottom of the lake decreased in areas where aquatic plants grew, and the total P during resuspension mainly comprised dissolved P. Fang's group [13] show that the level of turbulence decreased with upward seepage and reported lower P release and sediment resuspension in a tilting flume experiment. Jin et al. [14] showed that adsorption leads to a rapid decrease in the concentration of Zn^{2+} in the overlying water, and a lower final concentration is reached in a water flume experiment. However, note that studies based on experimental water flumes have limitations in terms of water depth, considering physically undisturbed sediments, and statistical parallelism. With advances in numerical simulation, the transport mechanism of the sediment-water interface has attracted attention as a multiple-field-based dynamic coupling mechanism. Voermans et al. [15] reported the existence of three transport regimes where molecular, dispersive, or turbulent transport dominates the mass flux across the sediment-water interface. Transitions between these regimes are defined by the permeability Reynolds number. Jiang et al. [16] explored the combined effects of mechanisms on the hyporheic exchange through laboratory experiments and numerical simulations involving an infiltrating solute that is displaced in a layered bedform with a low permeability layer. Cheng's group [17-19] proposed the release and diffusion law of sediment pollutants near the interface; moreover, the influence on water quality by factors such as turbidity, pollutants concentration, biochemical oxygen demand, and chemical oxygen demand of the overlying water was proposed under dynamic hydrodynamic conditions. In addition, in shallow waters, wind-induced waves are the main hydrodynamic factors determining sediment resuspension. Further, P is an important biogenic element in the aquatic ecosystem, and it provides nutrition for fish, algae, and other aquatic organisms. Multiple monitoring results have indicated that the adsorbed P concentration is much greater than that of dissolved P and that the adsorbed P is up to 90% of the total P in some cases. Tang et al. [20] proposed the wind speed could effectively trigger sediment resuspension, sediment resuspension significantly contributed to particulate nutrient release and impacted nutrient behavior. Huang et al. [21] reported the algal growth rate synchronically increased with dissolved total phosphorus (DTP) release rate after sediment resuspension. Due to the increase of dissolved alkaline phosphatase activity (DAPA) caused by sediment resuspension, a low to moderate disturbance is beneficial to algae growth. Because of the interaction between particles and water near the interface during the process of sediment resuspension, the local flow field and pressure fluctuation distribution are very complex, and the process of P release and transportation too is extremely complex. In this regard, field observation involves the qualitative analysis of the relationship between hydrodynamics and P concentration. Experimental measurement while maintaining the original state of P adsorption in the initial stage is difficult. The mechanisms of P release and transport during resuspension are not well understood. Based on experimental calibration parameters, numerical simulation has gradually become an important method for examining P release and transport mechanisms [16,19]. Through numerical simulation, the coupling mechanism of the overlying water, resuspension sediment, and adsorption-desorption may be further understood based on the dynamic release of P under wind-induced waves. The coupling mechanism of pollutant transport at the interface could help gain a deep and systematic understanding of the eutrophication mechanisms of large shallow lakes, and then it also could be an efficient means to understanding the change, structure, and functional response of the water ecosystem.

2. Surface pressure of wind-induced waves

The freshwater lakes in the middle and lower reaches of the Yangtze River in China are mainly shallow lakes. It has

sufficient fetch and a shallow water depth to allow frequent wind-, wave-, and current-generated events, which cause sediment resuspension. The significant wave height of wind-induced waves in shallow lakes is mainly affected by wind speed, water depth, and wind duration. At present, the main research methods for wind-induced waves are field observation, numerical simulation, and physical model experimentation. Field observation and model experimentation are important methods for the study of wind and waves in lakes. Based on long-term observation and experimental data, many achievements of engineering significance have been made. The influence of different water depths, wind speeds, and wind distances on the wind-induced wave was analyzed according to the experimental data of a wind-wave flume (60 m long, 0.8 m wide, and 1.2 m deep) [22]. The wind speed $\mathbf{U}_{z=0.1\text{ m}}$ is the average wind speed at a height of 0.1 m from the water surface. The relationship between wind speed ($\mathbf{U}_{z\ =\ 0.1\ \text{m}}$), water depth ($h$), wave height ($H$), and wavelength ($L$) is shown in Fig. 1. After the full development of wind-induced waves, the relative wave height (H/h) and wavelength (L/h) increased almost linearly with the dimensionless wind speed. In addition, H/L values were less than 1/20 under different wind speeds. Therefore, according to the linear wave theory, the potential function on the static water surface can be used instead of the potential function on the wave surface.

Based on the wave dispersion relation, the relationship among water depth, wave height, and wave period can be obtained

$$L = \frac{gT^2}{2\pi}\tanh\left(\frac{2\pi}{L}h\right), \tag{1}$$

where L is the wavelength, h is the water depth, and T is the wave period.

Based on the linear wave theory, the wave surface equation can be defined as follows:

$$\eta(x,t) = \frac{H}{2}\cos(kx-\omega t), \tag{2}$$

where H is the wave height, k and ω are the wavenumber and frequency, respectively, x is the horizontal movement distance, and t is the time.

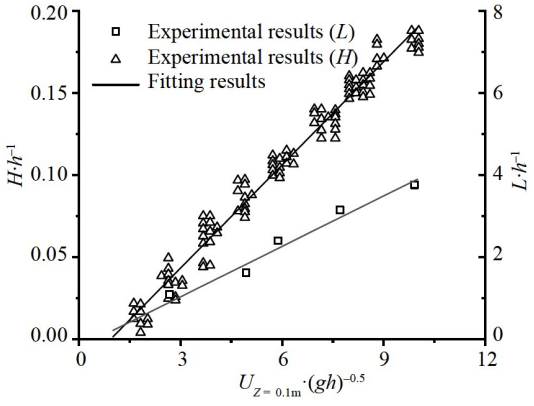

Figure 1 Relationship between wind speed and wave parameters.

According to the linearized dynamic conditions, the pressure distribution in the flow field can be obtained as follows:

$$p = \rho g\frac{\cosh k(z+h)}{\cosh kh}\eta - \rho g z, \tag{3}$$

where η is the wave surface equation, and z is the vertical depth. When $z = 0$, the pressure on the water surface can be obtained.

3. Numerical model

3.1 Governing equations

According to the previous experimental measurements, resuspended sediments contain a large number of fine particles, such as silt and clay. The median diameter D_{50} of the sediment is about 25-50 μm. It should be noted that the median diameter D_{50} of the upper sediment is less than 20 μm. In this study, D_{50} = 20 μm is selected as the representative particle size of the resuspended sediment. In the water-sediment-contaminant model, the mixed solution of resuspended sediment and water is considered as suspension, which may be due to the small particle size of sediment [23]. According to the experimental data of suspension [24,25], its viscosity can be considered as the equation of particle volume fraction. Thus, the suspension has macroscopic characteristics of a single fluid, such as density and viscosity.

The basic model assumptions are as follows.

(1) The density is considered constant in each phase.

(2) Each phase is considered to have the same pressure field.

(3) The particle relaxation time is considered to be much smaller than the macroscopic flow time.

For phase k, the mixture density of the suspension and the mixture velocity of suspension is defined as follows:

$$\rho_{\text{m}} = \sum_{k=1}^{n}\varphi_k\rho_k, \tag{4}$$

$$\mathbf{u}_{\text{m}} = \frac{1}{\rho_{\text{m}}}\sum_{k=1}^{n}\varphi_k\rho_k\mathbf{u}_k, \tag{5}$$

where φ_k is the particle volume fraction of a phase; ρ_k is the density of a phase; $\mathbf{u}_k$ is the velocity of a phase; ρ_{m} is the mixture density of the suspension; and $\mathbf{u}_{\text{m}}$ is the mixture velocity of suspension. Note that ρ_{m} varies though the component densities are constants.

Because the suspension can be considered as a continuous medium, the continuity equation of the suspension can be obtained as follows:

$$\frac{\partial\rho_{\text{m}}}{\partial t} + \rho_{\text{m}}\nabla\cdot\mathbf{u}_{\text{m}} = 0. \tag{6}$$

The momentum equation is obtained by summing over the phases for suspension flow.

$$\frac{\partial}{\partial t}\rho_{\mathrm{m}}\mathbf{u}_{\mathrm{m}}+\nabla\cdot\left(\rho_{\mathrm{m}}\mathbf{u}_{\mathrm{m}}\mathbf{u}_{\mathrm{m}}\right)=-\nabla p_{\mathrm{m}}+\nabla\cdot\boldsymbol{\tau}_{\mathrm{m}}+\nabla\cdot\boldsymbol{\tau}_{\mathrm{Dm}}+\rho_{\mathrm{m}}\mathbf{g}+\mathbf{M}_{\mathrm{m}},\tag{7}$$

where p_{m} is the mixture pressure. In practice, the phase pressures are often regarded as equal. $\boldsymbol{\tau}_{\mathrm{m}}$ is the sum of the turbulent stress and viscous stress, and $\boldsymbol{\tau}_{\mathrm{m}}=\mu_{\mathrm{m}}\boldsymbol{\gamma}_{\mathrm{m}}$ holds for a generalized Newtonian fluid. Further, $\mathbf{M}_{\mathrm{m}}$ is the influence of the surface tension force on the mixture. To simulate the flow fields, the standard k-ε turbulence model was used [26]. The model constants were obtained from the experimental data [27]: $C_{\mu}=0.09$, $\sigma_k=1.0$, $\sigma_{\varepsilon}=1.3$, $C_{\varepsilon 1}=1.44$, and $C_{\varepsilon 2}=1.92$.

The $\boldsymbol{\tau}_{\mathrm{Dm}}$ is defined by the following relation:

$$\boldsymbol{\tau}_{\mathrm{Dm}}=-\sum_{k=1}^{n}\varphi_k\rho_k\mathbf{u}_{\mathrm{M}k}\mathbf{u}_{\mathrm{M}k},\tag{8}$$

where $\mathbf{u}_{\mathrm{M}k}$ is the diffusion velocity, i.e., $\mathbf{u}_{\mathrm{M}k}=\mathbf{u}_k-\mathbf{u}_{\mathrm{m}}$.

The particle transport equation is determined as follows:

$$\frac{\partial}{\partial t}\varphi_k+\nabla\cdot\left(\varphi_k\mathbf{u}_{\mathrm{m}}\right)=-\nabla\cdot\mathbf{N}_k,\tag{9}$$

where $\mathbf{N}_k$ is the total diffusive flux resulting from two different mechanisms, namely [28], the flux generated by the gradients in the particle-particle collision, $\mathbf{N}_{kc}$, and a flux generated by gradients in suspension viscosity, $\mathbf{N}_{k\mu}$.

The concentration transport equation is determined as follows:

$$\frac{\partial c}{\partial t}+\mathbf{u}_{\mathrm{m}}\cdot\nabla c=\mathbf{D}\nabla^2 c+\mathbf{R},\tag{10}$$

where c is the concentration of concentration, $\mathbf{D}$ is the diffusion coefficient, $\mathbf{R}$ is the concentration generated or consumed in unit time and unit volume, which is the source and sink term.

Usually, the suspension viscosity ($D_{50}<0.1$ mm) is written as a function of the local particle volume fraction [29]. In this study, the particle volume fraction of the phase is only the sediment particle volume fraction, the Maron-Pierce-Quemada (MPQ) [24] model can be used for suspension.

$$\mu_{\mathrm{m}}=\mu_0\left(1-\frac{\varphi_k}{\varphi_{\max}}\right)^{-2},\tag{11}$$

where $\varphi_{\max}$ is the maximum concentration, which is about 0.62 for sediment particles.

3.2 Geometric model

The geometric model used in the numerical simulation refers to the wind-induced waves experiment (water depth h, 0.19 m; width, 0.80 m) [22]. The geometric model of the wave flume is divided into three areas, namely, the left, central, and right sides (Fig. 2). The left and right sides are the wave-eliminating areas, and the central area is the wind-induced wave action area. The sediment particles and P only exist in the middle area. The length of each of these areas is 6 times the wavelength. The origin of the coordinate system is the center of the upper surface, and the middle area of the wave flume is selected as the study object.

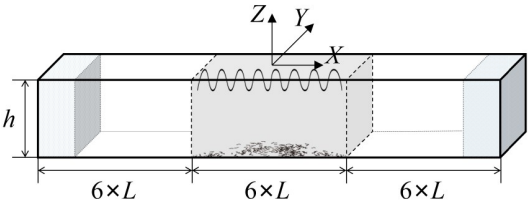

Figure 2 Computational domain for simulation.

3.3 Boundary and initial conditions

3.3.1 Flow-field boundary conditions

The bottom and wall of the wave flume are no-slip boundaries:

$$\mathbf{u}_{\mathrm{m}}=\mathbf{0}.\tag{12}$$

The top surface is a normal stress boundary, and the normal stress is p in the central area and 0 in the other areas:

$$p(x,t)=\rho g\frac{H}{2}\cos(kx-\omega t).\tag{13}$$

To avoid the reflection of waves at the left and right boundaries, damping wave-eliminating zones are set at the left and right boundaries of the wave flume by adding a damping source term to the momentum equation. This condition is expressed as follows:

$$\mathbf{S}=\beta\frac{x-x_1}{|x_1-x_2|}\mathbf{u}_{\mathrm{m}},\tag{14}$$

where x_1 is the starting point of the wave-eliminating zone; x_2 is the end of the wave-eliminating zone; β is the target variable [30], which is the weighted combination of the Reynolds-averaged Navier-Stokes equations (RANS) solution in the domain and the theoretical solution based on the boundary definition.

3.3.2 Transport-field boundary conditions

For the particle- and contaminant-transport field, in the central area, the wall and top surface of wave flume are set as no-flux boundaries:

$$\left.\begin{aligned}\mathbf{n}\cdot\left(\mathbf{u}_{\mathrm{m}}c-D\nabla c\right)=0,\\ \mathbf{n}\cdot\left(\mathbf{u}_{\mathrm{m}}\varphi_k-D\nabla\varphi_k\right)=0.\end{aligned}\right\}\tag{15}$$

The left and right boundaries are set as the periodic boundary conditions in the particle- and contaminant-transport field, i.e., the concentrations and volume fractions at the two boundaries are equal.

The bottom of the wave flume is a volume-fraction boundary and concentration boundary. Moreover, P adsorp-

tion on the particles reaches the maximum adsorption capacity.

3.3.3 *Initial conditions*

For the initial conditions, the initial pressure is related to the water depth (p_0 is the atmospheric pressure), the initial velocity is zero.

$$p = p_0 + \rho g(-z). \tag{16}$$

The particle size (D_{50}) of the sediment is 20 μm, and the initial sediment particle volume fraction of water is 0. The initial P concentration in water is 0.

The density of water is 997 kg/m^3, the density of sediment is 2650 kg/m^3, the viscosity of the overlying water is 1×10^{-3} Pa s.

3.4 Numerical method

In this study, the flow of the mixture of sediment particles and water was simulated by a sequential coupling method. First, the mixture flow under wind-induced waves in the flume was modeled in three dimensions using the RANS equations with the k-ε turbulence closure scheme, as solved by the finite volume method (OpenFOAM [31]). Second, according to the spatiotemporal distribution of the pressure and velocity conditions, the transport equation of P concentration, including the adsorption-desorption process, was established. The coupled flow field and P transport were then simulated within a Java Application Programming Interface (API) of COMSOL [16], which provides an easy and efficient way to implement the batch simulations. In particular, because the effect of sediment particles on density is much greater than that of P, the effect of P concentration on density is ignored in all cases. The resuspension process of the surface sediment is considered in the model, and the influence of the unknown heterogeneity caused by water content is ignored (i.e., the surface sediment in the model is assumed as homogeneous).

4. Model validation

The calculated and experimental sediment concentration distributions over the water depth, resulting from wave action, were compared. For numerical simulation, after the grid independence test, the 60 grids were divided within a unit wavelength, and the grids were refined with eight layers at the top surface. The five grids were divided within the unit wave height, and the time step was 1/100 of the wave period. The model validation was based on the measurement data of the suspended sediment concentration in a wave flume [32]. The calculated parameters are consistent with the experimental results as shown in Table 1.

Table 1 Calculation parameters for model validation

	h (m)	H (m)	T (s)	L (m)	D_{50} (μm)
Experiment 1 [32]	0.3	0.14	1.7	2.71	130
Experiment 2 [32]	0.3	0.09	1.7	2.71	97
Experiment 3 [32]	11.3	2.0	8	72.43	80

In Fig. 3, some calculated sediment concentration distributions over the water depth under wave action are given. Mostly great differences in concentrations are found between positions close to the bed and positions at higher levels. Therefore, the use of a logarithmic horizontal scale in diagrams like Fig. 3 seems appropriate. The vertical z-axis is linear; $z = 0$ is the water surface level, $z = -h$ is the bed level. In this study, the concentration of sediment will be further expressed in kg/m^3; this links up with the direct results of analyses of concentration measurements. The sediment concentration is non-linearly distributed in the vertical direction, higher near the bed and lower near the water surface. The numerical simulation results are in good agreement with the experimental results, and when the particle size is smaller, the calculated results are closer to the experimental results.

5. Results

Two types of cohesive fine sediments (D_{50}=20 μm) were selected: Sediment 1 and Sediment 2 came from Suzhou River and Guanting Reservoir [33], respectively. Based on the experimental measurements of P adsorption by sediment [19], the Langmuir adsorption isotherm, Eq. (17), was selected to fit the experimental data.

$$Q_a = \frac{Q_m K c}{1 + K c}, \tag{17}$$

where Q_a is the equilibrium adsorption capacity (mg/g); Q_m is the maximum adsorption capacity (mg/g); c is the concentration of P (mg/L) at equilibrium; K is the adsorption strength.

The primary form of P adsorption is the rapid physical adsorption of sediment particles, moreover, the adsorption and desorption occur rapidly. For Sediment 1, Q_m is 0.706 (mg/g), K is 1.139. For Sediment 2, Q_m is 0.422 (mg/g), K is 0.981. The correlation coefficients are 0.97 and 0.96, respectively. According to the experimental conditions [19,31], it is assumed that the sediment concentration near the sediment-water interface is 10 g/L, the phosphorus adsorption capacity reaches the maximum.

Based on the experimental measurements, the relationship between the characteristic wind speed (U_z = 0.1 m), water depth (h), wave height (H), wavelength (L), and wave period (T) is shown in Fig. 2. As mentioned earlier, two types of cohesive fine sediments were selected, i.e., Sediment 1 and

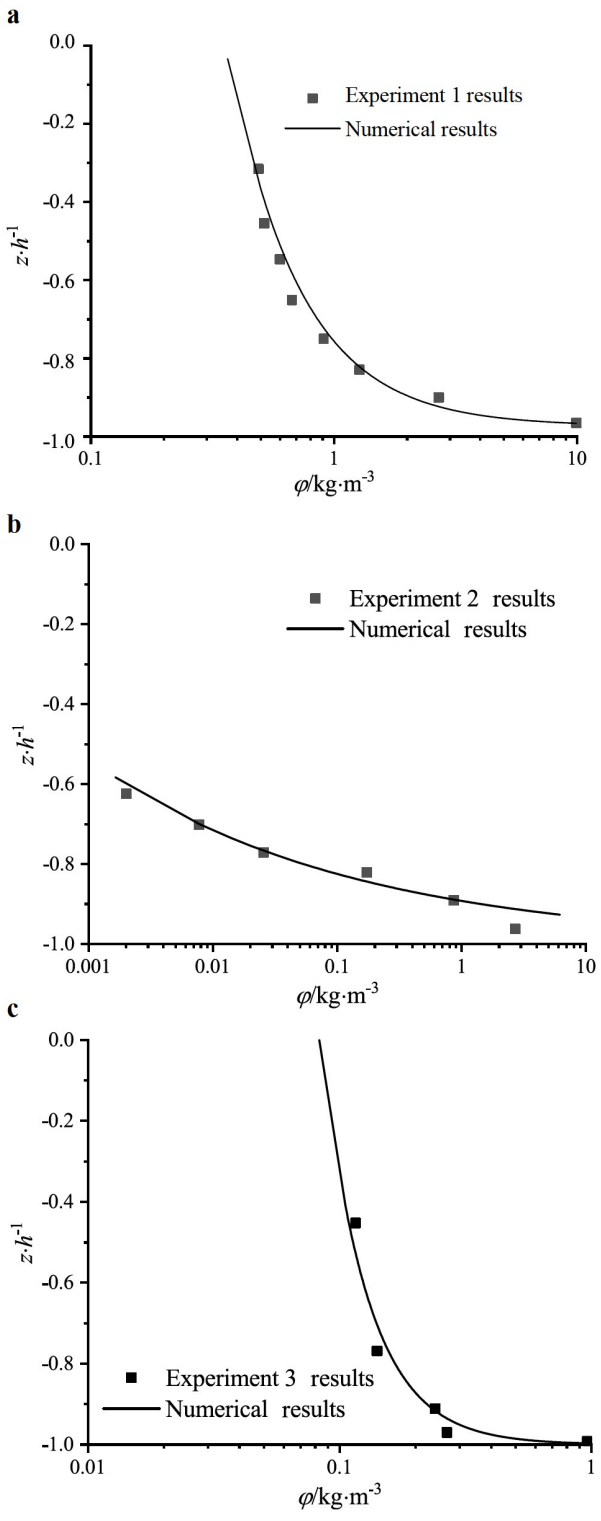

Figure 3 Comparison of the numerical simulation results and experimental results.

Sediment 2. The sediment concentration in a bed was 10 g/L. In this study, P concentration in the overlying water after sediments resuspension was calculated under different cases (Table 2). As seen from the data in Table 2, *H*/*L* values were less than 1/20 in different cases. Therefore, according to the linear wave theory, the potential function on the static water surface was used instead of the potential function on the wave surface.

Table 2 Calculation parameters for wind-induced waves

	$\mathbf{U}_{z=0.1}\cdot(\mathbf{g}h)^{-0.5}$	*T* (s)	*L* (m)	*H* (cm)	*H*/*L*
Case 1	2.92	0.35	0.19	0.73	0.039
Case 2	5.36	0.49	0.38	1.66	0.044
Case 3	7.80	0.61	0.57	2.59	0.045
Case 4	10.24	0.73	0.76	3.51	0.046

With the development of wind-induced waves, Fig. 4 shows the pressure distribution in the overlying water for different wave periods. At low wind speeds, the pressure of overlying water caused by wind-induced waves changes slightly, and the surface pressure of the overlying water changes periodically, while the pressure near the sediment-water interface is almost constant. Under high wind speeds, the pressure of the overlying water caused by wind-induced waves is effectively transferred to the interface, and the pressure near the interface exhibits periodicity. When the wind-induced waves are fully developed (100 *T*), the sediment is resuspended and enters the overlying water, causing a gradual increase in the sediment concentration near the interface. This results in a change in the density and viscosity of the mixture near the interface and in turn change the pressure and local flow fields near the interface.

The energy of wind-induced waves is mainly determined by wind speed. With an increase in wind speed, the pressure increases non-linearly near the sediment-water interface, as shown in Fig. 5. Initially, the interface pressure increases slowly with wind speed, and as seen from Cases 2, 3, and 4, it is higher than that in Case 1 by 1.07%, 3.24%, and 5.94%, respectively. After the wind-induced wave is fully developed, the interface pressure increases significantly with wind speed, and an increase of 3.59%, 8.05%, and 14.65% were observed in Cases 2, 3, and 4 compared with Case 1. In addition, in Cases 1-4, the pressure near the interface increases by 4.84%, 7.45%, 9.73%, and 13.46%, respectively, after full development. The shear stress near the interface increased from 0.02 to 0.04 Pa. Thus, under a high wind speed, the resuspended sediment causes a clear change in the interface pressure distribution.

The suspended sediment under wind-induced waves is mainly generated by the combined action of convective diffusion and turbulent diffusion caused by the pressure fluctuation near the sediment-water interface. The vertical distributions of the average volume fraction (φ) of particles in the overlying water at different time (Fig. 6) for different cases are similar under different wind speed conditions. Owing to the short-period reciprocating flow of wind-induced waves, the distribution is lower near the overlying water surface and the highest near the interface.

At relatively low wind speed, the wave height of the water

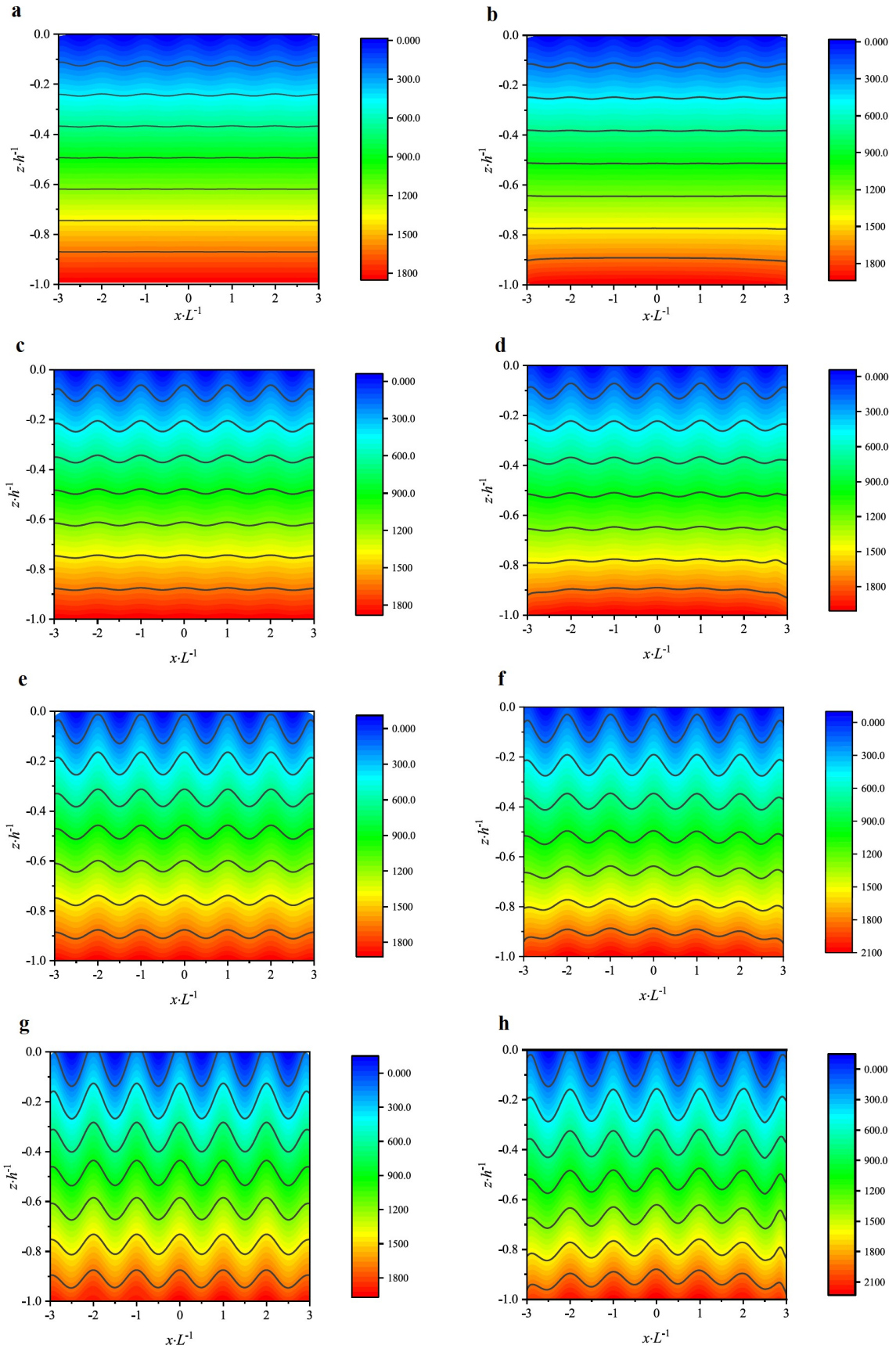

Figure 4 Pressure distribution for different wave periods.

surface and the pressure fluctuation at the interface is small. The sediment leaps into the overlying water periodically in the form of sediment clouds, and the φ of the particles in the overlying water gradually stabilizes with a small fluctuation. At high wind speeds, the wave height of the water surface and the pressure fluctuation of the interface is large. Then, the sediment near the interface moves in a layer-by-layer manner, and a thin layer near the interface results in high-intensity sediment transport. The sediment leaps into the overlying water in the form of a burst, and the φ of the particles in the overlying water increases gradually with fluctuations.

After full development of the wind-induced waves, the φ value in the overlying water increases greatly with an increase in wind speed at different locations, as shown in Fig. 7. The increase in φ in the overlying water is related to the periodic movement of water and depends on the convection and diffusion caused by wind-induced waves. The uniformity of φ is positively correlated with the intensity of convection. Therefore, the higher the wind speed, the more uniform the φ distribution is. The total amount of φ can be obtained by integration. The total amount of φ in Cases 2, 3, and 4 are 0.63, 1.28, and 2.19 times, respectively, of the total φ in Case 1.

Based on the monitoring results of P in natural water, the total amount of dissolved P is much lower than that of adsorbed P. According to the characteristics of physical adsorption, the adsorbed P can be rapidly desorbed and released from sediment after the resuspension of sediments; moreover, the total amount of P increases greatly in the

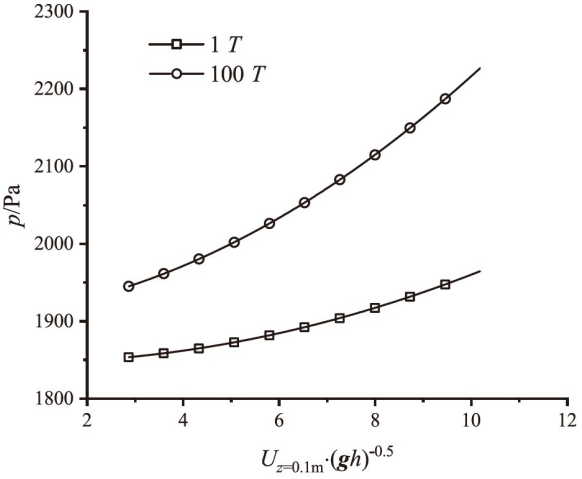

Figure 5 Peak pressure with wind velocity at different time.

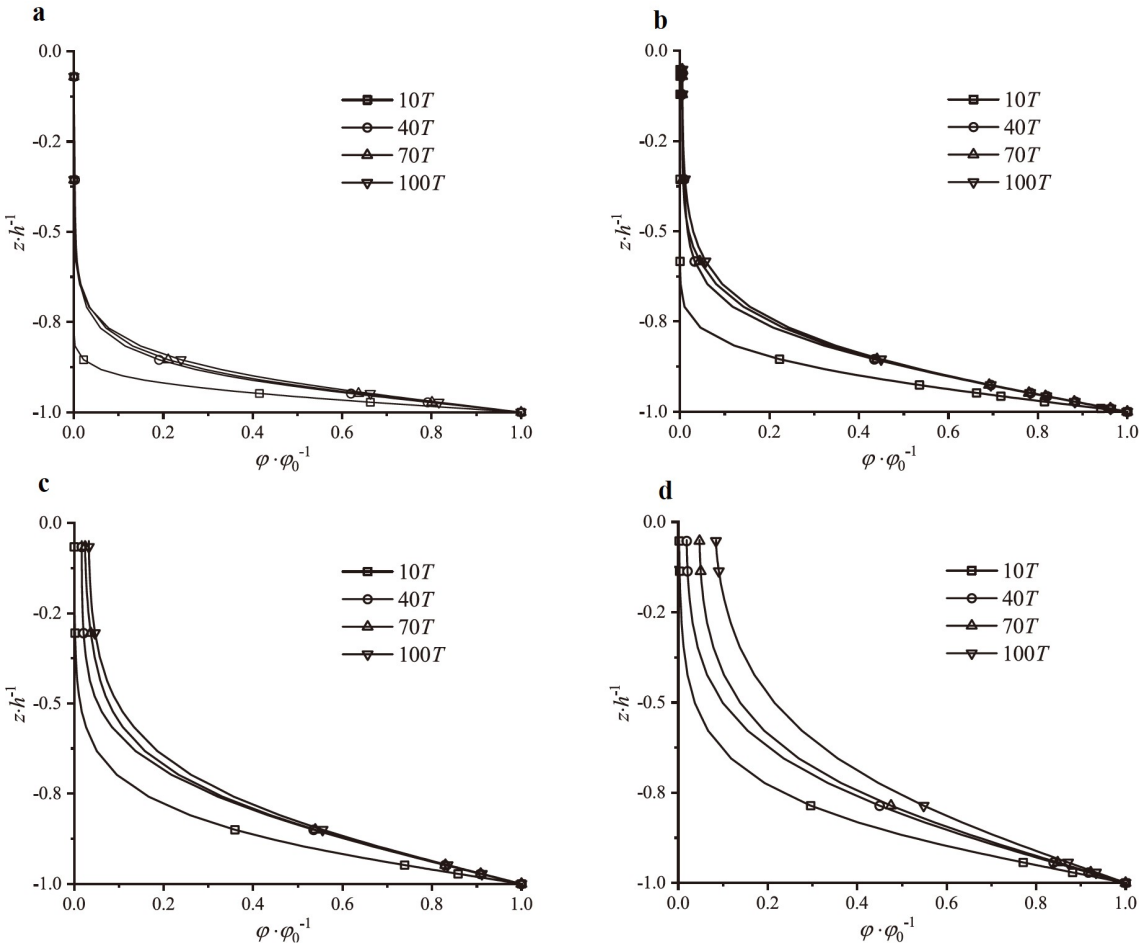

Figure 6 Vertical distributions of average volume fraction (φ) of particles in the overlying water at different time.

overlying water, causing secondary pollution of water. Both, Sediment 1 and Sediment 2 with different adsorption-desorption characteristics were analyzed. As shown in Fig. 8, for Cases 1-4, the average total P concentration (c) changes with time. Under different wind-induced waves, c gradually reaches equilibrium at a low wind speed in the overlying water, while that increases at a high wind speed in the overlying water. Thus, fluctuations occur during the increase. There exists an inflection point during the increase in c. Before this inflection point, i.e., when the wind-induced wave begins to develop, c increases rapidly. The time taken to reach the inflection point is positively related to the wind speed.

From Cases 1-4, the wind speed increases by ~3.5 times, while c in the overlying water for Sediment 1 and Sediment 2 significantly increases to ~2.53 and ~2.39 times, respectively. With the development of wind-induced waves, the φ in the overlying water tends to be more or less constant at low wind speeds, and c tends to be stable. Under high wind speeds, φ in the overlying water increases significantly, and c also increases rapidly. With an increase in wind speed, the rates of increase of c for Sediment 1 and Sediment 2 become relatively close after the different sediment resuspension. However, because of the different adsorption-desorption capacities of Sediment 1 and Sediment 2, c in water changes by more than 40%. This difference is negatively correlated with the wind speed; as the wind speed increases, the difference decreases from 52% to 43%. Therefore, the change in c attributed to the adsorption-desorption capacity is more sensitive to low wind speed, and that caused by wind speed is

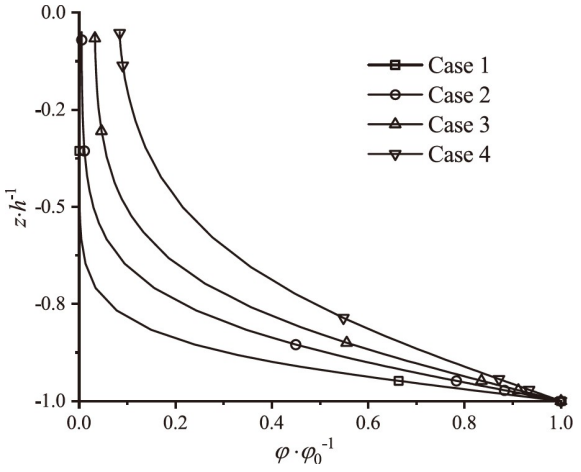

Figure 7 Vertical distribution of φ in overlying water at 100T.

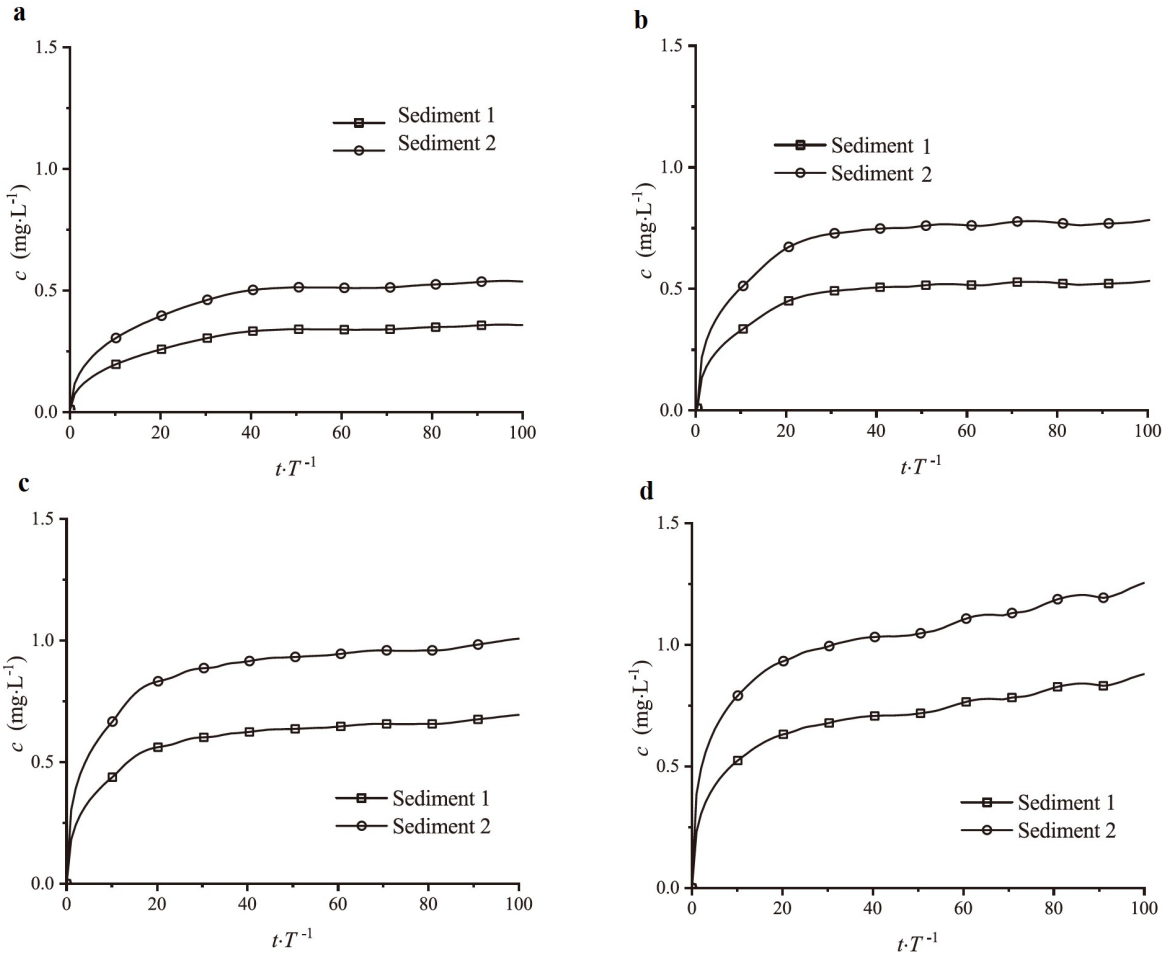

Figure 8 Relationship between the average total P concentration and time.

more sensitive to high wind speed.

For sediments with different adsorption-desorption capacities, the amount of P released per unit of sediment (c/φ) also varies with the wind-induced waves, as shown in Fig. 9. In the initial stage of resuspension, the concentration of P in overlying water is low, and P concentrations differ greatly between phases. The P desorbed by the particles is quickly released into the water, resulting in a rapid increase in the concentration of P in the water. With a gradual increase in P concentration in the overlying water, the difference in P concentrations between the phases decreases gradually, and the desorption-release amount of each particle also gradually decreases. For the sediment with low adsorption-desorption capacity (Sediment 1), c/φ did not change much with wind speed and wave period. For the sediment with high adsorption-desorption capacity (Sediment 2), c/φ did not vary greatly with wave period at low wind speeds but decreased rapidly with wave period at high wind speeds. Meanwhile, the c/φ of the two sediments decreased with an increase in wind speed. After the wind-induced waves were fully developed, c/φ was negatively correlated with wind speed.

The initial and final values of c/φ are compared in Fig. 10. When the wind-induced wave begins to develop, c/φ increases slightly with the wind speed. After the full development of the wind-induced wave, c/φ decreases by 19.5% and 27.1% with wind speed for Sediment 1 and Sediment 2, respectively. For Sediment 1, the equilibrium between P concentration and sediment adsorption capacity is attained rapidly, and c/φ is not sensitive to wind speed. For Sediment 2, the adsorption capacity is stronger, and the P concentration in water and sediment adsorption capacity reaches equilibrium slower than in the case of Sediment 1 and changes with the dynamic resuspension of sediment; c/φ is more sensitive to wind speed in the case of Sediment 2.

6. Conclusions

Based on the experimental and coupled numerical simulation results, the relationships among wind speed, wavelength, wave height, wave period, pressure, sediment volume fraction, total P concentration, and unit sediment desorption release were examined. The main conclusions of this work are as follows.

Wind speed directly affects the wind-induced waves. With the increase in wind speed, the wave height on the water surface gradually increases, and pressure near the sediment-water interface increases non-linearly. Simultaneously, owing to the mass transport at the interface, the pressure near the interface increases further after the wind-induced wave develops. The resuspended sediment causes clear changes in the pressure distribution near the interface under high wind speeds.

When the wind speed is relatively low, the sediment periodically leaps into the overlying water in the form of a sediment cloud, and the φ in the overlying water gradually reaches a stable value with small fluctuations. At higher wind speeds, the sediment near the interface moves in layers, and high-intensity sediment transport occurs near the interface. The sediment bursts into the overlying water and the φ in the overlying water increases significantly with fluctua-

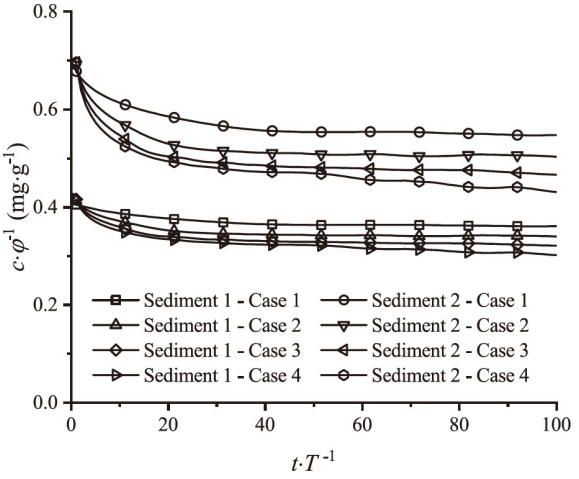

Figure 9 Relationship between the amount of P released per unit of sediment (c/φ) and time.

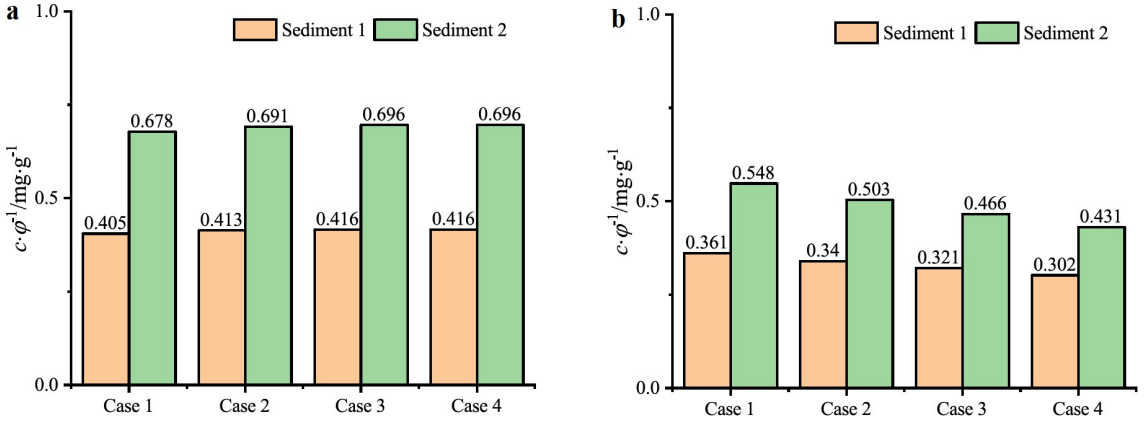

Figure 10 Comparison of the initial and final values of c/φ.

tions. The increase in φ far away from the interface is related to the periodic movement of water caused by wind-induced waves.

Under different wind-induced waves, the total P concentration in the overlying water gradually reaches equilibrium at low wind speeds, while it increases with fluctuations at high wind speeds. Because of the different adsorption-desorption capacities of the two types of Sediment considered, the corresponding total P concentrations differed by more than 40%. For the sediment with high adsorption-desorption capacity, c/φ did not vary greatly with wave period at low wind speeds but decreased rapidly with wave period at high wind speeds. After the development of wind-induced waves, c/φ was negatively correlated with wind speed.

In shallow waters, low and intermediate wind speeds are common. When sediments with high adsorption capacity are resuspended by small-scale flow-field changes, the P concentration in the overlying water increases abruptly and is difficult to diffuse. Then, the release of P exhibits the characteristics of concentrated release in a small region. The DAPA increases with time, which provided the enzyme for hydrolyzing a variety of organic phosphorus compounds. The increase of DAPA is one of the important factors affecting the eutrophication mechanism of large shallow lakes. Therefore, in areas with strong sediment adsorption, monitoring should be strengthened and biological or chemical P removal measures could be adopted to reduce the risk of environmental problems such as water bloom. In addition, under the low and intermediate wind speeds, the released P is difficult to diffuse. Hence, it can be speculated that the chemical P removal effect is better than that under static or high wind speeds.

The study of pollutant transport at the interface can help gain a deep and systematic understanding of the change, structure, and functional response of aquatic ecosystems. Knowledge of the coupling transport mechanism may provide important insights into the restoration of polluted shallow lakes or rivers. An important research direction for the future is to elucidate the interactions of wind-induced waves and deep sediments. Unlike in the case of surface sediments, the water content of deep sediments gradually decreases, and rheological properties such as yield strength should be considered during resuspension, which may lead to a large change in P in local areas.

This work was supported by the Strategic Priority Research Program of the National Key R&D Program of China (Grant Nos. 2018YFC1505500, and 2018YFC1505504), and the National Natural Science Foundation of China (NSFC) (Grant Nos. 11802313, and 12032005).

1 P. Cheng, H. Zhu, B. Zhong, and D. Wang, Transport mechanisms of contaminants released from fine sediment in rivers, Acta Mech. Sin. **31**, 791 (2015).

2 C. Fan, Advances and prospect in sediment-water interface of lakes: A review, J. Lake Sci. **31**, 1191 (2019).

3 K. J. Fetters, D. M. Costello, C. R. Hammerschmidt, and G. A. Burton Jr., Toxicological effects of short-term resuspension of metal-contaminated freshwater and marine sediments, Environ Toxicol Chem **35**, 676 (2016).

4 G. Matisoff, S. B. Watson, J. Guo, A. Duewiger, and R. Steely, Sediment and nutrient distribution and resuspension in Lake Winnipeg, Sci. Total Environ. **575**, 173 (2017).

5 H. Lepage, M. Launay, J. Le Coz, H. Angot, C. Miège, S. Gairoard, O. Radakovitch, and M. Coquery, Impact of dam flushing operations on sediment dynamics and quality in the upper Rhône River, France, J. Environ. Manage. **255**, 109886 (2020).

6 M. Pivato, L. Carniello, J. Gardner, S. Silvestri, and M. Marani, Water and sediment temperature dynamics in shallow tidal environments: The role of the heat flux at the sediment-water interface, Adv. Water Resources **113**, 126 (2018).

7 S. L'Helguen, L. Chauvaud, P. Cuet, P. Frouin, J. F. Maguer, and J. Clavier, A novel approach using the 15n tracer technique and benthic chambers to determine ammonium fluxes at the sedimentwater interface and its application in a back-reef zone on reunion island (Indian ocean), J. Exp. Mar. Biol. Ecol. **452**, 143 (2014).

8 J. Y. Xue, X. Y. Jiang, X. L. Yao, M. Li, L. Zhang, Dissimilatory nitrate reduction processes at the sediment-water interface in lake Kuilei, China Environ. Sci. **38**, 2289 (2018).

9 N. Zaaboub, A. Ounis, M. A. Helali, B. Béjaoui, A. I. Lillebø, E. F. Silva, and L. Aleya, Phosphorus speciation in sediments and assessment of nutrient exchange at the water-sediment interface in a mediterranean lagoon: Implications for management and restoration, Ecol. Eng. **73**, 115 (2014).

10 G. W. Zhu, B. Q. Qin, L. Zhang, L. C. Luo, X. g. Sun, D. L. Hong, Y. J. Gao, and R. Xie, Wave effects on nutrient release of sediments from Lake Taihu by flume experiments, J. Lake Sci. **17**, 61 (2005).

11 B. You, T. Wang, C. Fan, Quantitative simulative method of sediment resuspension in Lake Taihu, J. Lake Sci. 19, 611 (2007).

12 D. Wu, and Z. Hua, The effect of vegetation on sediment resuspension and phosphorus release under hydrodynamic disturbance in shallow lakes, Ecol. Eng. **69**, 55 (2014).

13 A. Sharma, L. Huang, H. Fang, and X. Li, Effects of hydrodynamic on the mobility of phosphorous induced by sediment resuspension in a seepage affected alluvial channel, Chemosphere **260**, 127550 (2020).

14 G. Jin, Z. Zhang, R. Li, C. Chen, H. Tang, L. Li, and D. A. Barry, Transport of zinc ions in the hyporheic zone: Experiments and simulations, Adv. Water Resour. **146**, 103775 (2020).

15 J. J. Voermans, M. Ghisalberti, and G. N. Ivey, A model for mass transport across the sediment-water interface, Water Resour. Res. **54**, 2799 (2018).

16 Q. Jiang, G. Jin, H. Tang, C. Shen, M. Cheraghi, J. Xu, L. Li, and D. A. Barry, Density-dependent solute transport in a layered hyporheic zone, Adv. Water Resour. **142**, 103645 (2020).

17 H. W. Zhu, D. Z. Wang, P. D. Cheng, J. Y. Fan, and B. C. Zhong, Effects of sediment physical properties on the phosphorus release in aquatic environment, Sci. China-Phys. Mech. Astron. **58**, 1 (2015).

18 H. W. Zhu, P. D. Cheng, W. Li, J. H. Chen, Y. Pang, and D. Z. Wang, Empirical model for estimating vertical concentration profiles of resuspended, sediment-associated contaminants, Acta Mech. Sin. **33**, 846 (2017).

19 P. Cheng, X. Wang, and C. Feng, Numerical simulation of phosphorus release from resuspended sediment, Acta Mech. Sin. **36**, 1191 (2020).

20 C. Tang, Y. Li, C. He, and K. Acharya, Dynamic behavior of sediment resuspension and nutrients release in the shallow and wind-exposed Meiliang Bay of Lake Taihu, Sci. Total Environ. **708**, 135131 (2020).

21 J. Huang, Q. Xu, B. Xi, X. Wang, W. Li, G. Gao, S. Huo, X. Xia, T. Jiang, D. Ji, H. Liu, and K. Jia, Impacts of hydrodynamic disturbance on sediment resuspension, phosphorus and phosphatase release, and cyanobacterial growth in Lake Tai, Environ. Earth Sci. **74**, 3945

(2015).
22 C.-Z. Yuan, T.-Q. Hu, Y.-X. You, Experimental study on the characteristics of wind-induced waves in shallow water, Chin. J. Hydrodyn. **29**, 536 (2014).
23 H. M. Shewan, and J. R. Stokes, Analytically predicting the viscosity of hard sphere suspensions from the particle size distribution, J. Non-Newtonian Fluid Mech. **222**, 72 (2015).
24 J. J. Stickel, and R. L. Powell, Fluid mechanics and rheology of dense suspensions, Annu. Rev. Fluid Mech. **37**, 129 (2005).
25 E. J. Hinch, The measurement of suspension rheology, J. Fluid Mech. **686**, 1 (2011).
26 B. E. Launder, and D. B. Spalding, The numerical computation of turbulent flows, Comput. Methods Appl. Mech. Eng. **3**, 269 (1974).
27 D. C. Wilcox, Turbulence Modeling for CFD, 3rd ed (DCW Industries Inc., La Canada Flintridge, 2010).
28 I. R. Siqueira, and P. R. de Souza Mendes, On the pressure-driven flow of suspensions: Particle migration in apparent yield-stress fluids, J. Non-Newtonian Fluid Mech. **265**, 92 (2019).
29 C. I. Mendoza, and I. Santamaría-Holek, The rheology of hard sphere suspensions at arbitrary volume fractions: An improved differential viscosity model, J. Chem. Phys. **130**, 044904 (2009).
30 N. G. Jacobsen, D. R. Fuhrman, and J. Fredsøe, A wave generation toolbox for the open-source CFD library: OpenFoam®, Int. J. Numer. Meth. Fluids **70**, 1073 (2012).
31 Z. Deng, P. Wang, and P. Cheng, Hydrodynamic performance of an asymmetry OWC device mounted on a box-type breakwater, Front. Mar. Sci. **8**, 677030 (2021).
32 J. Van de Graaff, Sediment Concentration due to Wave Action. Dissertation for Doctoral Degree (Delft University of Technology, Delft, 1988).
33 M.-H. Chen, The Phosphorus Adsorption Rule and Surface Microtopography Change of Sediment Particle, Dissertation for Doctoral Degree (Tsinghua University, Beijing, 2008).

浅水风生波作用下再悬浮沉积物中磷释放的研究

程鹏达, 朱心广, 安翼, 冯春

摘要 沉积物-水界面是湖泊的重要界面, 与大多数环境和生态问题有关. 风生波引起沉积物再悬浮造成水体二次污染. 由于水、再悬浮沉积物和磷的耦合机制会影响界面附近磷的释放, 因此探索了两种不同吸附-解吸能力沉积物的耦合模型, 以检查沉积物再悬浮后磷的释放规律. 得到了风速、风生波特性、沉积物分布和水体含磷量之间的关系. 风生波影响沉积物-水界面附近的局部流场, 造成沉积物再悬浮. 对于不同的沉积物, 单位沉积物解吸释放量与风速呈负相关. 中低风速时, 沉积物因界面小范围流场变化再悬浮, 上覆水中的磷快速增加, 且难于扩散. 此时, 磷的释放表现出小范围集中释放的特点, 可能迅速影响水环境, 也可能为治理提供了窗口期.